Combined computational and cellular screening identifies synergistic inhibition of SARS-CoV-2 by lenvatinib and remdesivir

Marie O. Pohl[a,*], Idoia Busnadiego[a,*], Francesco Marrafino[b], Lars Wiedmer[b], Annika Hunziker[a], Sonja Fernbach[a], Elena Omori[b], Benjamin G. Hale[a], Amedeo Caflisch[b,§] & Silke Stertz[a,§]

[a]Institute of Medical Virology, University of Zurich, Winterthurerstrasse 190, 8057 Zurich, Switzerland.

[b]Department of Biochemistry, University of Zurich, Winterthurerstrasse 190, 8057 Zurich, Switzerland.

[*] These authors contributed equally.

[§] To whom correspondence should be addressed: caflisch@bioc.uzh.ch or stertz.silke@virology.uzh.ch

ABSTRACT

Rapid repurposing of existing drugs as new therapeutics for COVID-19 has been an important strategy in the management of disease severity during the ongoing SARS-CoV-2 pandemic. Here, we screened by high-throughput docking 6,000 compounds within the DrugBank library for their potential to bind and inhibit the SARS-CoV-2 3CL main protease, a chymotrypsin-like enzyme that is essential for viral replication. For 19 candidate hits, parallel *in vitro* fluorescence-based protease-inhibition assays and Vero-CCL81 cell-based SARS-CoV-2 replication-inhibition assays were performed. One hit, diclazuril (an investigational anti-protozoal compound), was validated as a SARS-CoV-2 3CL main protease inhibitor *in vitro* (IC50 value of 29 μM) and modestly inhibited SARS-CoV-2 replication in Vero-CCL81 cells. Another hit, lenvatinib (approved for use in humans as an anti-cancer treatment), could not be validated as a SARS-CoV-2 3CL main protease inhibitor *in vitro*, but serendipitously exhibited a striking functional synergy with the approved nucleoside analogue remdesivir to inhibit SARS-CoV-2 replication in Vero-CCL81 cells. Lenvatinib is a broadly-acting host receptor tyrosine kinase (RTK) inhibitor, but the synergistic effect with remdesivir was not observed with other approved RTK inhibitors (such as pazopanib or sunitinib), suggesting that the mechanism-of-action is independent of host RTKs. Furthermore, time-of-addition studies revealed that lenvatinib/remdesivir synergy probably targets SARS-CoV-2 replication subsequent to host-cell entry. Our study shows that combining computational and cellular screening is an efficient means to identify existing drugs with repurposing potential as antiviral compounds. Future studies should aim at understanding and optimizing the lenvatinib/remdesivir synergistic mechanism as a therapeutic option.

44 **IMPORTANCE**

45 Successful repurposing of existing drugs as COVID-19 therapeutics would be a rapid and
46 important means to limit disease severity during the SARS-CoV-2 pandemic. In this study,
47 we used a computational screening approach to identify existing drugs that might inhibit
48 the function of a critical enzyme (the 3CL main protease) encoded by the causative agent
49 of COVID-19, SARS-CoV-2. While we found that diclazuril (an investigational human drug
50 already approved for use in animals) inhibited this viral enzyme *in vitro*, it only showed
51 modest ability to inhibit SARS-CoV-2 replication in cells. However, our approach
52 serendipitously identified lenvatinib (an anti-cancer drug approved for use in humans) as
53 a potent inhibitor of SARS-CoV-2 replication when combined with the existing approved
54 antiviral drug, remdesivir. Our findings raise the possibility that future studies to
55 understand the molecular mechanisms underlying the lenvatinib/remdesivir synergy could
56 uncover new therapeutic principles for treatment of COVID-19 or similar viral diseases.

57

58 **INTRODUCTION**

59 Severe acute respiratory syndrome coronavirus 2 (SARS-CoV-2) entered the human
60 population in late 2019 and rapidly spread around the globe causing a devastating
61 pandemic with significant impacts on human health and the worldwide economy (1, 2).
62 Infection with SARS-CoV-2 results in a respiratory disease, COVID-19, that is mild in most
63 individuals or even asymptomatic. However, in vulnerable patients, in particular in
64 individuals with compromised immune systems, such as the elderly or
65 immunosuppressed, the virus can cause a severe life-threatening pneumonia (2-4). Thus,
66 large efforts have been undertaken to develop vaccines and antiviral drugs for the
67 prevention and treatment of COVID-19. While several vaccines have been developed and
68 licensed at unprecedented speeds, the development of antiviral drugs has not yet been
69 successful (5-8). Remdesivir is the only antiviral drug that is currently approved and used
70 to treat COVID-19 patients in many countries, but its efficacy has been questioned by
71 recent results from a large-scale clinical trial (9, 10). Thus, additional efforts are urgently
72 needed to fill this gap.

73 Early on in the pandemic, drug development approaches focused on the repurposing of
74 drugs approved for other conditions as a means to accelerate the process of bringing drug
75 candidates to market (11, 12). One of the viral drug targets that has gained particular
76 interest is the SARS-CoV-2 protease, 3CL M^{pro}, a chymotrypsin-like protease that cleaves
77 the two polyproteins, pp1a and pp1ab, and is essential for viral replication (13, 14). 3CL
78 M^{pro} is considered a promising target for drug development as its structure has been
79 solved and there is no homologous human protease (15, 16). Moreover, protease
80 inhibitors have been developed successfully to treat HIV-1 and hepatitis C virus infections

81 (17, 18). While several inhibitors of 3CL M^{pro} have already been identified, no drug
82 targeting 3CL M^{pro} has been approved yet (15, 19-22). Here, we computationally screened
83 a library of approved drugs for novel 3CL M^{pro} inhibitors. The identified drug candidates
84 were then tested for their antiviral potential in an *in vitro* 3CL M^{pro} protease-inhibition
85 assay, and in a Vero cell-based virus replication assay using authentic SARS-CoV-2.
86 While two potential inhibitors (diclazuril and ramelteon) identified *in silico* possessed
87 modest antiviral activity, we found that lenvatinib, an inhibitor of receptor tyrosine kinases
88 such as vascular endothelial growth factor receptors, displayed strong synergistic
89 inhibition of SARS-CoV-2 with the approved drug remdesivir.

90

91 **RESULTS**

92 To identify novel inhibitors of the SARS-CoV-2 3CL M^{pro}, we performed an *in silico*
93 screening campaign of the Drugbank library which contains approximately 6000 approved
94 drugs (23). The docking was carried out by the computer program SEED (details in
95 Methods section) using two holo structures of 3CL M^{pro} (PDB codes 5r82 and 5re9). The
96 binding pocket was considered rigid during docking. The calculation of the binding energy
97 makes use of a force field-based methodology. Upon filtering and ranking, the top 19
98 compounds were purchased for experimental validation (Fig. 1A, B).

99 An *in vitro* fluorescence-based protease-inhibition assay with recombinant 3CL M^{pro}
100 protease was employed to measure the potential inhibition of enzymatic activity by each
101 compound. The positive control, GC376, was used as reference compound (22). An IC_{50}
102 (inhibitor concentration that results in 50% reduction of activity with respect to buffer-only
103 solution) value of 316 nM was measured for GC376, which is consistent with a reported

104 value of 190 nM (22). First, single-dose measurements were carried out at 100 μM for
105 each compound (Fig. 1C). For only two compounds a substantial reduction (> 40% with
106 respect to DMSO-only) of 3CL M^{pro} activity was measured. In follow-up dose-response
107 experiments with these two compounds, diclazuril showed an IC_{50} of 29 μM, and
108 oprea1_409650 showed an IC_{50} of 100 μM (Fig. 1D, E). The binding mode of diclazuril as
109 predicted by docking is shown in Figure 1F.

110 In parallel, we tested the 19 predicted 3CL M^{pro} protease inhibitors for their potential to
111 inhibit SARS-CoV-2 replication in Vero CCL81 cells. Following pretreatment with the
112 different inhibitors for 2 h, Vero CCL81 cells were infected with SARS-CoV-2 isolate
113 SARS-CoV-2/human/Switzerland/ZH-395-UZH-IMV5/2020 at a multiplicity of infection
114 (MOI) of 0.01 PFU/cell and viral titers were determined at 24 h post-infection. Remdesivir,
115 a known inhibitor of SARS-CoV-2 (24), was included as a positive control. In parallel,
116 inhibitor-treated cells were left uninfected and cell viability was determined. With the
117 exception of compounds 9-aminocampthecin and 1-deazaadenosine, cell viability was
118 only minimally affected by treatment with the inhibitors (Fig. 2A). In line with previous
119 reports, SARS-CoV-2 replication was inhibited by remdesivir in a dose-dependent
120 manner, thus validating our screening assay (Fig. 2B). We also observed significant
121 inhibition of virus replication with three of the predicted protease inhibitors, lenvatinib,
122 ramelteon and diclazuril (Fig. 2B). Of note, diclazuril, which was the most potent protease
123 inhibitor in the *in vitro* protease assay, was also the strongest hit in the screen for inhibition
124 of SARS-CoV-2 replication. Oprea1, which also displayed inhibition in the protease assay
125 did not reduce viral replication significantly. While the inhibitory effects of the three hit
126 compounds were robust and reproducible across the replicates of the SARS-CoV-2
127 screening assay, the degree of inhibition was only around 50-60% and thus modest (Fig.

128 2C). In order to test whether the inhibitors would show greater antiviral potential when
129 combined with an established inhibitor of SARS-CoV-2, we tested them in combination
130 with low concentrations of remdesivir. While ramelteon and diclazuril did not increase virus
131 inhibition by remdesivir, the combination of remdesivir and lenvatinib showed a very strong
132 synergistic effect: the low concentration of remdesivir used reduced viral titers
133 approximately 3-fold, but in combination with lenvatinib, SARS-CoV-2 titers were reduced
134 >1000-fold (Fig. 2D), which was not due to cytotoxic effects (Supp. Fig. 1A). When the
135 three hit compounds were tested in human Calu-3 cells for their impact on SARS-CoV-2
136 replication, we did not detect any effect on cell viability (Supp. Fig. 1B) but also no
137 inhibition of virus growth, either by the inhibitors alone or in combination with low doses of
138 remdesivir (Supp. Fig. 1C). Thus, the striking synergistic effect of lenvatinib in combination
139 with remdesivir appears to be specific to Vero CCL81 cells.

140 As lenvatinib did not inhibit SARS-CoV-2 3CL M^{pro} in the *in vitro* protease-inhibitor assay
141 at the concentration used in cell culture-based assays (Fig. 1C), we speculated that its
142 function as an inhibitor of receptor tyrosine kinases (RTKs) might contribute to the
143 observed synergy with remdesivir. We therefore selected pazopanib and sunitinib as
144 additional RTK inhibitors to test for synergy with remdesivir, as they exhibit a similar
145 inhibition profile to lenvatinib, with all three shown to inhibit vascular endothelial growth
146 factor receptors (VEGFR1, VEGFR2 and VEGFR3), platelet-derived growth factor
147 receptor (PDGFR-a/-b), and c-Kit with comparable specificity and potency (25, 26). When
148 taking cell viability into consideration, only lenvatinib displayed a clear synergistic effect
149 with remdesivir (Fig. 2E, Supp. Fig. 1D) suggesting that the observed synergistic inhibitory
150 effect is not linked to inhibition of VEGFR-, PDGFR- or c-Kit induced signaling. Next, we
151 performed a time-of-addition experiment, in which we treated cells with remdesivir,

152 lenvatinib, or the combination of both inhibitors, at 1 h prior to infection, 1 h post infection,
153 or 4 h post infection. At 24 h post infection, supernatants were harvested and infectious
154 virus titers determined by plaque assay. As expected from an RNA polymerase inhibitor,
155 remdesivir retained its antiviral potential if given post viral entry: treatment with remdesivir
156 1 h post infection resulted in a similar inhibition of virus replication as treatment of cells
157 prior to infection (Fig. 2F). In addition, treatment with remdesivir at 4 h post infection still
158 led to a substantial decrease in viral replication. The synergistic effect of lenvatinib and
159 remdesivir was highly similar for pretreatment and 1 h post-treatment conditions, both
160 resulting in potent inhibition of virus replication. Furthermore, the 4 h post infection
161 treatment condition resulted in a less potent, but still substantial, decrease in viral titers
162 by more than 10-fold (Fig. 2F). Thus, our data suggest that the synergistic effect of
163 lenvatinib and remdesivir could be due to more potent inhibition of the viral transcription
164 and/or replication processes rather than any effects on earlier stages of the viral
165 replication cycle.

166

167 **DISCUSSION**

168 Our approach of combining *in silico* and *in vitro* screenings of an approved drug library for
169 inhibitors of the SARS-CoV-2 3CL M^{pro} protease identified diclazuril as a low micromolar
170 inhibitor of the 3CL M^{pro} protease, and three drugs (diclazuril, ramelteon, and lenvatinib)
171 that reduced viral replication in Vero CCL81 cells. Moreover, lenvatinib showed an
172 unexpectedly strong synergy with remdesivir. This shows that the approach used here
173 can identify compounds with antiviral potential.

174 There are several caveats to the approach adopted in this study. Of note, we only tested
175 the compounds at a single 10 μM concentration, and thus an immediate option to see
176 stronger inhibition of virus replication would be to test higher concentrations of the
177 inhibitors. However, this might result in the identification of additional compounds with
178 antiviral potential but only in a non-physiologically achievable range of concentrations.
179 Thus, extensive compound modification and optimization for increased antiviral potential
180 would be required in subsequent studies and would slow immediate roll-out of a
181 repurposed drug. Given that our goal was to rapidly identify approved drugs as treatment
182 options for COVID-19 and circumvent the lengthy process of progressing inhibitors to
183 approval, we set the threshold at 10 μM and did not consider higher drug concentrations.
184 Options to improve the yield of our screening approach could be to use an alternative
185 structure of 3CL M^{pro} that was subsequently solved by room temperature X-ray
186 crystallography (27). It reveals the ligand-free structure of the active site and the
187 conformation at near-physiological temperature, and was suggested to be a better target
188 for *in silico* screening for inhibitors of 3CL M^{pro} (27). Moreover, additional libraries of
189 approved drugs could be included, for example IUPHAR/BPS
190 (https://www.guidetopharmacology.org/) and ChEMBL (https://www.ebi.ac.uk/chembl/),
191 although they overlap substantially with DrugBank.
192 A second caveat is the apparent cell-type specificity of synergy observed between
193 lenvatinib and remdesivir: this effect was clear in Vero CCL81cells, but not in human Calu-
194 3 cells. One possible explanation could be that lenvatinib inhibits a Vero cell-specific target
195 that is not inhibited in Calu-3 cells. This could either be due to differential expression levels
196 of the respective target or could be related to differences in target sequence and structure
197 between the human and the African green monkey version of the target. As the conversion

198 of remdesivir to its active metabolite (remdesivir triphosphate) is less efficient in Vero
199 CCL81 cells as compared to Calu-3 cells (24), the synergistic effect of lenvatinib with
200 remdesivir could be linked to the metabolic conversion of remdesivir. If lenvatinib
201 treatment led to a higher conversion rate, and thus to higher levels of the active metabolite
202 of remdesivir it could be hypothesized that in Calu-3 cells, where the conversion of
203 remdesivir to remdesivir triphosphate is already efficient, an increase in conversion
204 efficiency would not result in a boost of the antiviral potential of remdesivir. However, it is
205 thus far unclear how lenvatinib would affect the metabolic conversion of remdesivir. Given
206 that lenvatinib did not significantly inhibit the SARS-CoV-2 3CL M^{pro} protease in the *in vitro*
207 protease assay, the known targets of lenvatinib (i.e. receptor tyrosine kinases (RTKs),
208 such as VEGFR, PDGFR or c-Kit), could be the relevant drug targets for inhibition of virus
209 replication and synergy with remdesivir. We did not observe synergy for two other RTK
210 inhibitors with comparable RTK specificity and potency, and thus the observed synergy is
211 probably not mediated by inhibition of VEGFRs, PDGFRs or c-Kit, which are targeted by
212 all three inhibitors. Thus, future work should aim to reveal the mechanism behind the
213 synergistic action of remdesivir and lenvatinib. Such studies on the Vero cell-specific
214 synergy could reveal broader insights into the metabolism and antiviral mechanism of
215 nucleoside analogs and thus aid the development of antiviral drugs.
216

217 **MATERIALS AND METHODS**

218 ***In silico* screen for 3CL M^{pro} inhibitors.** The evaluation of the binding energy by the
219 program SEED makes use of a force field-based energy function. Protein and ligand
220 electrostatic desolvation penalties are approximated by a continuum dielectric treatment

221 and the generalized Born model (28-30). The partial charges and vdW parameters for the
222 atoms in the protein and in the ligands were taken from the CHARMM36 all-atom force
223 field and the CHARMM general force field (CGenFF), respectively (31-33). Importantly,
224 CHARMM36 and CGenFF employ a consistent paradigm for the determination of partial
225 charges and vdW parameters. The dielectric discontinuity surface was approximated by
226 the molecular surface. The dielectric constant was assigned a value of 2.0 and 78.5 for
227 the volume occupied by the solute and solvent, respectively. Default SEED parameters
228 were used. The nearly 6000 approved and experimental drugs in DrugBank with more
229 than 17 non-hydrogen atoms were docked by SEED. This filter on molecular sizes was
230 employed to avoid the selection of very small molecules which cannot provide sufficient
231 affinity. SEED offers three methods for the actual placement of the fragments: (1) polar
232 docking in which fragments are positioned and oriented such that at least one favorable
233 hydrogen bond with a residue in the binding site is formed, (2) apolar docking in which
234 fragments are placed in the hydrophobic regions of the binding site, and (3) a combination
235 of (1) and (2). The latter placement procedure was used. The docking was carried out on
236 two holo structures of 3CL M^{pro} (PDB codes 5r82 and 5re9) with high resolution. The
237 residue Glu166 was selected for the definition of the binding pocket. For PDB 5r82 no
238 water molecules were retained, while for PDB 5re9 one buried water molecule was
239 retained. Two energy filters were used: total binding energy < -10 kcal/mol and van der
240 Waals efficiency < -1.0 kcal/mol per non-hydrogen atom. Hydrogen bonding penalty was
241 calculated for each compound, according to the method described by Zhao and Huang
242 (34). If newly formed hydrogen bonds between the ligand and the protein are not in good
243 geometry or desolvated donors/acceptors are not involved into new hydrogen bonds, an
244 enthalpic loss arises due to uncompensated breakage of hydrogen bonds with waters.

245 The hydrogen bonding penalty index is calculated by checking both the solvation and
246 hydrogen bonding state of donors/acceptors at the protein-ligand interface. A value of 1
247 in penalty corresponds to about 1.5 kcal/mol in binding free energy. This penalty can then
248 be integrated into total binding energy values according to the formula SEED total energy
249 + hydrogen bonding penalty*1.5kcal/mol. Compounds were then ranked by recalculated
250 total energy and heavy atom count. Up to top five compounds for each heavy atom count
251 tier were selected and experimental phase drugs were removed, focusing on approved
252 drugs. The resulting compounds were visually inspected, favoring compounds that
253 established H-bonds, and 19 compounds in total were selected.

254 ***In vitro* protease inhibition assay.** The in vitro inhibition assay was based on
255 fluorescence and was carried out according to the specifications of the vendor (Reaction
256 Biology, Catalogue #: Mpro). The assay measures the inhibitory activity of compounds
257 that compete with a known peptide substrate for purified 3CL Mpro. The peptide contains
258 a quencher and a donor group, thus fluorescence is quenched in an intact peptide. Upon
259 cleavage of the peptide by 3CL Mpro the donor fragment generates fluorescence which
260 is quantified by a luminometer. The fluorogenic substrate used is [NH2-
261 C(EDANS)VNSTQSGLRK(DABCYL)M-COOH]. The positive control is GC376 which was
262 employed as reference compound. Single-dose screenings were performed at 100 μM.

263 **Compound screening for inhibitors of SARS-CoV-2.** To test the selected compounds
264 from the docking analysis for antiviral activity against SARS-CoV-2, $1.2x10^4$ Vero CCL81
265 cells were seeded in DMEM supplemented with 10% fetal calf serum (FCS), 100 U/ml of
266 penicillin, and 100 μg/ml of streptomycin in 96-well plates and incubated overnight at 37°C
267 and 5% CO_2. For the infection and cell viability experiments, compound dilutions of 10 μM

268 and a final DMSO concentration of 0.1% were used. As negative control, 0.1% DMSO
269 was used while 10, 5 and 2.5 µM remdesivir (at a final DMSO concentration of 0.1%)
270 served as positive controls. The day after seeding, cells were washed with PBS followed
271 by incubation with the individual compounds at a concentration of 10 µM diluted in Opti-
272 MEM (Gibco) for 2 h at 37°C and 5% CO_2. Next, medium was removed and cells were
273 infected with SARS-CoV-2 (SARS-CoV-2/human/Switzerland/ZH-395-UZH-IMV5/2020)
274 at a multiplicity of infection (MOI) of 0.01 PFU/cell diluted in PBS supplemented with 0.3%
275 BSA, 1 mM Ca^{2+}/Mg^{2+}, 100 U/ml penicillin, and 100 µg/ml streptomycin (35). Cells were
276 then incubated for 1 h at 37°C and 5% CO_2. Following infection, the inoculum was
277 removed and DMEM supplemented with 10 µM of the respective compound (or the
278 positive or negative control), 100 U/ml penicillin, 100 µg/ml streptomycin, 0.3% BSA,
279 20 mM HEPES, 0.1% FCS, and 0.5 µg/ml TPCK-treated trypsin was added to the cells.
280 After incubation for 24 h at 37°C and 5% CO_2, cell supernatants were harvested and virus
281 titer was determined by plaque assay.

282 In parallel to the infection experiments, cell viability following incubation of Vero CCL81
283 cells with the respective compounds was assessed using the same experimental set-up
284 as for the infection experiments but instead of infection with SARS-CoV-2, cells were
285 mock-infected with PBS supplemented with 0.3% BSA, 1 mM Ca^{2+}/Mg^{2+}, 100 U/ml
286 penicillin, and 100 µg/ml streptomycin for 1 h at 37°C and 5% CO_2. Cell viability was
287 determined 24 h after the addition of compound-containing DMEM using the CellTiterGlo
288 kit (Promega) and a luminescence plate reader (Perkin Elmer). The infection and cell
289 viability experiments for the compound screen were performed in duplicates in three
290 independent experiments.

291 For the analysis of the compound screen, all titers were normalized to the negative control
292 (0.1% DMSO) and log2-transformed. Next, the z-score was calculated by dividing the
293 difference of the normalized and transformed titer of a given sample and the average
294 normalized and transformed titer of the negative control by the standard deviation of the
295 normalized and transformed negative control (36). The average z-score of the three
296 independent replicates for a given sample was used for hit selection. Compounds
297 associated with a z-score of smaller than -2 were considered as hits for further analysis.
298 Compounds associated with an average reduction in cell viability of more than 20%
299 relative to the negative control were not considered as hits.

300 **Testing for synergistic inhibition of SARS-CoV-2.** Vero CCL81 cells were seeded in
301 96 well plates at a density of 1.2 x 10^4 cells/well and incubated overnight. Cells were
302 washed once with PBS and incubated for 2 h at 37°C and 5% CO_2 with Opti-MEM (Gibco)
303 containing 5 or 2.5 µM remdesivir alone or in combination with 10 µM ramelteon
304 (PubChem ID 208902), lenvatinib (PubChem ID 9823820), diclazuril (PubChem ID
305 25273624), pazopanib (LC laboratories, P-6706) or sunitinib (Selleckchem, S1042) at a
306 final concentration of 0.1 % DMSO. DMSO 0.1 % was used as negative control. Cells
307 were infected with SARS-CoV-2 (SARS-CoV-2/human/Switzerland/ZH-395-UZH-
308 IMV5/2020) at a MOI of 0.01 in PBS supplemented with 0.3% BSA, 1 mM Ca^{2+}/Mg^{2+}, 100
309 U/ml penicillin, 100 µg/ml streptomycin. After 1 h at 37°C and 5% CO_2, cells were washed
310 once in PBS and the indicated compounds were added in Dulbecco's modified Eagle's
311 medium (DMEM; Gibco) supplemented with 100 U/ml penicillin, 100 µg/ml streptomycin,
312 0.3% BSA, 20 mM HEPES, 0.1 % FCS and 0.5 µg/ml TPCK-treated trypsin. Samples
313 were taken at 48 h post infection and supernatants were stored at -80°C prior to titer

314 determination by plaque assay. In parallel to the infection experiments, cell viability was
315 assessed as indicated in the compound screen section above. All experiments were
316 performed in duplicates in three independent experiments.

317 **Time of addition experiments.** Vero CCL81 cells were seeded in 96 well plates at a
318 density of 1.2 x 10^4 cells/well. After incubation overnight, cells were washed once with
319 PBS and incubated for 1 h at 37°C and 5% CO_2 with Opti-MEM (Gibco) containing the
320 indicated inhibitors. DMSO 0.1 % was used as negative control. Cells were infected with
321 SARS-CoV-2 (SARS-CoV-2/human/Switzerland/ZH-395-UZH-IMV5/2020) at a MOI of
322 0.01 PFU/cell in PBS supplemented with 0.3% BSA, 1 mM Ca^{2+}/Mg^{2+}, 100 U/ml penicillin,
323 100 µg/ml streptomycin. Following infection, the inoculum was removed and DMEM
324 supplemented with 100 U/ml penicillin, 100 µg/ml streptomycin, 0.3% BSA, 20 mM
325 HEPES, 0.1% FCS, and 0.5 µg/ml TPCK-treated trypsin was added to the cells. To test
326 for time of addition effect, the indicated compounds were added either 1 or 4 h post
327 infection instead of 1 h before infection in parallel samples. After incubation for 24 h at
328 37°C and 5% CO_2, cell supernatants were harvested, and virus titer was determined by
329 plaque assay. In parallel to the infection experiments, cell viability was assessed as
330 indicated above. All experiments were performed in duplicates in three independent
331 experiments.

332

333 **ACKNOWLEDGMENTS**

334 Work in the Stertz and Hale groups is supported by the Swiss National Science
335 Foundation (grant numbers 31003A_176170 (to SSt) and 31003A_182464 (to BGH)). The

336 Caflisch group is supported by an Excellence grant of the Swiss National Science
337 Foundation (310030B_189363).
338

339 **FIGURE LEGENDS**

340 **Fig. 1 *In silico* screen reveals novel inhibitors of the SARS-CoV-2 3CL M^{pro} protease.**
341 **A)** Schematic overview of the *in silico* screen by high-throughput docking for repurposing
342 known drugs. **B)** List of 19 compounds identified as potential inhibitors of 3CL M^{pro}. **C)**
343 The 19 compounds were tested in an *in vitro* fluorescence-based assay at a concentration
344 of 100 μM for their potential to inhibit 3CL M^{pro}. Mean values from three independent
345 results are shown with error bars representing standard deviations. GC376 is the positive
346 control. **D-E)** The two compounds that showed a reduction of enzymatic activity of more
347 than 40% (relative to DMSO solution) in the *in vitro* protease assay, oprea1_409650 (D)
348 and diclazuril (E), were tested at varying concentrations to obtain a dose-response curve.
349 Average values from three independent experiments are plotted with error bars
350 representing standard deviations. **F)** Predicted binding mode of diclazuril (carbon atoms
351 in magenta) to 3CL M^{pro} (ribbon model in cyan with the side chains of the catalytic dyad
352 in yellow). The hydrogen bonds between diclazuril and the backbone polar groups of
353 Glu166 are shown (dotted lines).

354 **Fig. 2. Lenvatinib acts synergistically with remdesivir to inhibit SARS-CoV-2. A)**
355 **Effect of inhibitor-treatment on cell viability.** Vero CCL81 cells were pre-treated for 2
356 h with 10 μM of a putative 3CL M^{pro} inhibitor or with DMSO 0.1% or RDV (10, 5, and 2.5
357 μM) as negative and positive control, respectively. Then, cells were mock-infected for 1 h
358 followed by incubation in the presence of the respective inhibitors or controls. 24 h after

359 mock-infection cell viability was assessed. Shown are means and standard deviation of
360 cell viability normalized to the DMSO control (depicted as a square) of three independent
361 experiments each performed in duplicates. RDV-treated cells are depicted as triangles.
362 Compounds reducing cell viability more than 20% compared to the DMSO control (marked
363 in red) were excluded from the selection. **B) Effect of inhibitor-treatment on SARS-**
364 **CoV-2 growth.** Experimental set-up as in A) but cells were infected with SARS-CoV2
365 (MOI=0.01) for 1 h followed by incubation in the presence of the respective inhibitors or
366 controls. After 24 h of incubation, cell supernatants were harvested and viral growth was
367 assessed by plaque assay. Virus titers of three independent experiments, each performed
368 in duplicate, were normalized to the DMSO control, log2-transformed and converted into
369 z-scores. Z-score of DMSO and RDV-treated cells are depicted as square and triangle,
370 respectively. Excluded inhibitors are marked in red. A z-score of smaller than -2 was used
371 for the selection of inhibitors for follow-up. **C) Normalized virus titers for selected**
372 **inhibitors.** Experimental set-up as in B). Shown are virus titers normalized to DMSO
373 control of the selected inhibitors from B). Depicted are means and standard deviation of
374 three independent experiments, each performed in duplicates. **D) Effect of combination**
375 **of selected inhibitors with RDV on SARS-CoV-2 growth.** Vero CCL81 cells were pre-
376 treated for 2 h with 10 µM of ramelteon, lenvatinib, or diclazuril combined with either 5 or
377 2.5 µM RDV. DMSO 0.1% or RDV (5 and 2.5µM) were used as negative and positive
378 control, respectively. Following infection with SARS-CoV-2 (MOI=0.01) for 1 h, cells were
379 incubated in the presence of the respective inhibitors or controls. After 48 h of incubation,
380 cell supernatants were harvested and viral growth was assessed by plaque assay. Shown
381 are mean virus titers and standard deviation of three independent experiments, each
382 performed in duplicate. **E) Effect of VEGFR inhibitors and RDV on SARS-CoV-2**

383 **growth.** Vero CCL81 cells were pre-treated for 2 h with lenvatinib (10 μM), pazopanib (10
384 μM), or sunitinib (1 μM) in combination with RDV (5 μM). DMSO 0.1% or RDV (5 μM) were
385 used as negative and positive controls, respectively. Following infection with SARS-CoV2
386 (MOI=0.01) for 1 h, cells were incubated in the presence of the respective inhibitors or
387 controls. After 48 h of incubation, cell supernatants were harvested and viral growth was
388 assessed by plaque assay. Shown are mean virus titers and standard deviation of three
389 independent experiments, each performed in duplicate. **F) Effect of time of addition on**
390 **the synergistic reduction of SARS-CoV-2 growth by lenvatinib and RDV.** Vero CCL81
391 cells were treated either 1 h before (-1h), 1 h after (+1h) or 4 h after (+4h) infection with
392 SARS-CoV-2 (MOI=0.01) with 10 μM of lenvatinib combined with either 5 or 2.5 μM RDV.
393 DMSO 0.1% or RDV (10, 5 and 2.5μM) were used as negative and positive control,
394 respectively. 24 h post infection, cell supernatants were harvested and viral growth was
395 assessed by plaque assay. Shown are mean virus titers and standard deviation of three
396 independent experiments, each performed in duplicates. LoD, limit of detection.

397

398

399 **REFERENCES**

400 1. Dong E, Du H, Gardner L. 2020. An interactive web-based dashboard to track COVID-19
401 in real time. Lancet Infect Dis 20:533-534.

402 2. Zhu N, Zhang D, Wang W, Li X, Yang B, Song J, Zhao X, Huang B, Shi W, Lu R, Niu P,
403 Zhan F, Ma X, Wang D, Xu W, Wu G, Gao GF, Tan W, China Novel Coronavirus I,
404 Research T. 2020. A Novel Coronavirus from Patients with Pneumonia in China, 2019. N
405 Engl J Med 382:727-733.

406 3. Wu Z, McGoogan JM. 2020. Characteristics of and Important Lessons From the
407 Coronavirus Disease 2019 (COVID-19) Outbreak in China: Summary of a Report of 72314
408 Cases From the Chinese Center for Disease Control and Prevention. JAMA 323:1239-
409 1242.

410 4. Huang C, Wang Y, Li X, Ren L, Zhao J, Hu Y, Zhang L, Fan G, Xu J, Gu X, Cheng Z, Yu
411 T, Xia J, Wei Y, Wu W, Xie X, Yin W, Li H, Liu M, Xiao Y, Gao H, Guo L, Xie J, Wang G,
412 Jiang R, Gao Z, Jin Q, Wang J, Cao B. 2020. Clinical features of patients infected with
413 2019 novel coronavirus in Wuhan, China. Lancet 395:497-506.

414 5. Polack FP, Thomas SJ, Kitchin N, Absalon J, Gurtman A, Lockhart S, Perez JL, Perez
415 Marc G, Moreira ED, Zerbini C, Bailey R, Swanson KA, Roychoudhury S, Koury K, Li P,
416 Kalina WV, Cooper D, Frenck RW, Jr., Hammitt LL, Tureci O, Nell H, Schaefer A, Unal S,
417 Tresnan DB, Mather S, Dormitzer PR, Sahin U, Jansen KU, Gruber WC, Group CCT. 2020.
418 Safety and Efficacy of the BNT162b2 mRNA Covid-19 Vaccine. N Engl J Med 383:2603-
419 2615.

420 6. Baden LR, El Sahly HM, Essink B, Kotloff K, Frey S, Novak R, Diemert D, Spector SA,
421 Rouphael N, Creech CB, McGettigan J, Khetan S, Segall N, Solis J, Brosz A, Fierro C,
422 Schwartz H, Neuzil K, Corey L, Gilbert P, Janes H, Follmann D, Marovich M, Mascola J,
423 Polakowski L, Ledgerwood J, Graham BS, Bennett H, Pajon R, Knightly C, Leav B, Deng
424 W, Zhou H, Han S, Ivarsson M, Miller J, Zaks T, Group CS. 2021. Efficacy and Safety of
425 the mRNA-1273 SARS-CoV-2 Vaccine. N Engl J Med 384:403-416.

426 7. Voysey M, Clemens SAC, Madhi SA, Weckx LY, Folegatti PM, Aley PK, Angus B, Baillie
427 VL, Barnabas SL, Bhorat QE, Bibi S, Briner C, Cicconi P, Collins AM, Colin-Jones R,
428 Cutland CL, Darton TC, Dheda K, Duncan CJA, Emary KRW, Ewer KJ, Fairlie L, Faust
429 SN, Feng S, Ferreira DM, Finn A, Goodman AL, Green CM, Green CA, Heath PT, Hill C,
430 Hill H, Hirsch I, Hodgson SHC, Izu A, Jackson S, Jenkin D, Joe CCD, Kerridge S, Koen A,
431 Kwatra G, Lazarus R, Lawrie AM, Lelliott A, Libri V, Lillie PJ, Mallory R, Mendes AVA,
432 Milan EP, Minassian AM, et al. 2021. Safety and efficacy of the ChAdOx1 nCoV-19 vaccine
433 (AZD1222) against SARS-CoV-2: an interim analysis of four randomised controlled trials
434 in Brazil, South Africa, and the UK. Lancet 397:99-111.

435 8. Krammer F. 2020. SARS-CoV-2 vaccines in development. Nature 586:516-527.

436 9. Consortium WHOST, Pan H, Peto R, Henao-Restrepo AM, Preziosi MP, Sathiyamoorthy
437 V, Abdool Karim Q, Alejandria MM, Hernandez Garcia C, Kieny MP, Malekzadeh R, Murthy
438 S, Reddy KS, Roses Periago M, Abi Hanna P, Ader F, Al-Bader AM, Alhasawi A, Allum E,
439 Alotaibi A, Alvarez-Moreno CA, Appadoo S, Asiri A, Aukrust P, Barratt-Due A, Bellani S,
440 Branca M, Cappel-Porter HBC, Cerrato N, Chow TS, Como N, Eustace J, Garcia PJ,
441 Godbole S, Gotuzzo E, Griskevicius L, Hamra R, Hassan M, Hassany M, Hutton D,
442 Irmansyah I, Jancoriene L, Kirwan J, Kumar S, Lennon P, Lopardo G, Lydon P, Magrini N,
443 Maguire T, Manevska S, et al. 2021. Repurposed Antiviral Drugs for Covid-19 - Interim
444 WHO Solidarity Trial Results. N Engl J Med 384:497-511.

445 10. Beigel JH, Tomashek KM, Dodd LE, Mehta AK, Zingman BS, Kalil AC, Hohmann E, Chu
446 HY, Luetkemeyer A, Kline S, Lopez de Castilla D, Finberg RW, Dierberg K, Tapson V,
447 Hsieh L, Patterson TF, Paredes R, Sweeney DA, Short WR, Touloumi G, Lye DC,
448 Ohmagari N, Oh MD, Ruiz-Palacios GM, Benfield T, Fatkenheuer G, Kortepeter MG, Atmar
449 RL, Creech CB, Lundgren J, Babiker AG, Pett S, Neaton JD, Burgess TH, Bonnett T,
450 Green M, Makowski M, Osinusi A, Nayak S, Lane HC, Members A-SG. 2020. Remdesivir
451 for the Treatment of Covid-19 - Final Report. N Engl J Med 383:1813-1826.

452 11. Riva L, Yuan S, Yin X, Martin-Sancho L, Matsunaga N, Pache L, Burgstaller-Muehlbacher
453 S, De Jesus PD, Teriete P, Hull MV, Chang MW, Chan JF, Cao J, Poon VK, Herbert KM,
454 Cheng K, Nguyen TH, Rubanov A, Pu Y, Nguyen C, Choi A, Rathnasinghe R, Schotsaert
455 M, Miorin L, Dejosez M, Zwaka TP, Sit KY, Martinez-Sobrido L, Liu WC, White KM,
456 Chapman ME, Lendy EK, Glynne RJ, Albrecht R, Ruppin E, Mesecar AD, Johnson JR,
457 Benner C, Sun R, Schultz PG, Su AI, Garcia-Sastre A, Chatterjee AK, Yuen KY, Chanda
458 SK. 2020. Discovery of SARS-CoV-2 antiviral drugs through large-scale compound
459 repurposing. Nature 586:113-119.

460 12. Gordon DE, Hiatt J, Bouhaddou M, Rezelj VV, Ulferts S, Braberg H, Jureka AS, Obernier
461 K, Guo JZ, Batra J, Kaake RM, Weckstein AR, Owens TW, Gupta M, Pourmal S, Titus
462 EW, Cakir M, Soucheray M, McGregor M, Cakir Z, Jang G, O'Meara MJ, Tummino TA,
463 Zhang Z, Foussard H, Rojc A, Zhou Y, Kuchenov D, Huttenhain R, Xu J, Eckhardt M,
464 Swaney DL, Fabius JM, Ummadi M, Tutuncuoglu B, Rathore U, Modak M, Haas P, Haas
465 KM, Naing ZZC, Pulido EH, Shi Y, Barrio-Hernandez I, Memon D, Petsalaki E, Dunham A,
466 Marrero MC, Burke D, Koh C, Vallet T, et al. 2020. Comparative host-coronavirus protein
467 interaction networks reveal pan-viral disease mechanisms. Science 370.

468 13. V'Kovski P, Kratzel A, Steiner S, Stalder H, Thiel V. 2020. Coronavirus biology and
469 replication: implications for SARS-CoV-2. Nat Rev Microbiol doi:10.1038/s41579-020-
470 00468-6.

471 14. Anand K, Ziebuhr J, Wadhwani P, Mesters JR, Hilgenfeld R. 2003. Coronavirus main
472 proteinase (3CLpro) structure: basis for design of anti-SARS drugs. Science 300:1763-7.

473 15. Zhang L, Lin D, Sun X, Curth U, Drosten C, Sauerhering L, Becker S, Rox K, Hilgenfeld R.
474 2020. Crystal structure of SARS-CoV-2 main protease provides a basis for design of
475 improved alpha-ketoamide inhibitors. Science 368:409-412.

476 16. Douangamath A, Fearon D, Gehrtz P, Krojer T, Lukacik P, Owen CD, Resnick E, Strain-
477 Damerell C, Aimon A, Abranyi-Balogh P, Brandao-Neto J, Carbery A, Davison G, Dias A,
478 Downes TD, Dunnett L, Fairhead M, Firth JD, Jones SP, Keeley A, Keseru GM, Klein HF,
479 Martin MP, Noble MEM, O'Brien P, Powell A, Reddi RN, Skyner R, Snee M, Waring MJ,
480 Wild C, London N, von Delft F, Walsh MA. 2020. Crystallographic and electrophilic
481 fragment screening of the SARS-CoV-2 main protease. Nat Commun 11:5047.

482 17. Farnik H, Zeuzem S. 2012. New antiviral therapies in the management of HCV infection.
483 Antivir Ther 17:771-83.

484 18. Wensing AM, van Maarseveen NM, Nijhuis M. 2010. Fifteen years of HIV Protease
485 Inhibitors: raising the barrier to resistance. Antiviral Res 85:59-74.

486 19. Drayman N, Jones KA, Azizi SA, Froggatt HM, Tan K, Maltseva NI, Chen S, Nicolaescu V,
487 Dvorkin S, Furlong K, Kathayat RS, Firpo MR, Mastrodomenico V, Bruce EA, Schmidt MM,
488 Jedrzejczak R, Munoz-Alia MA, Schuster B, Nair V, Botten JW, Brooke CB, Baker SC,
489 Mounce BC, Heaton NS, Dickinson BC, Jaochimiak A, Randall G, Tay S. 2020. Drug
490 repurposing screen identifies masitinib as a 3CLpro inhibitor that blocks replication of
491 SARS-CoV-2 in vitro. bioRxiv doi:10.1101/2020.08.31.274639.

492 20. Hung HC, Ke YY, Huang SY, Huang PN, Kung YA, Chang TY, Yen KJ, Peng TT, Chang
493 SE, Huang CT, Tsai YR, Wu SH, Lee SJ, Lin JH, Liu BS, Sung WC, Shih SR, Chen CT,
494 Hsu JT. 2020. Discovery of M Protease Inhibitors Encoded by SARS-CoV-2. Antimicrob
495 Agents Chemother 64.

496 21. Fu L, Ye F, Feng Y, Yu F, Wang Q, Wu Y, Zhao C, Sun H, Huang B, Niu P, Song H, Shi
497 Y, Li X, Tan W, Qi J, Gao GF. 2020. Both Boceprevir and GC376 efficaciously inhibit
498 SARS-CoV-2 by targeting its main protease. Nat Commun 11:4417.

499 22. Vuong W, Khan MB, Fischer C, Arutyunova E, Lamer T, Shields J, Saffran HA, McKay RT,
500 van Belkum MJ, Joyce MA, Young HS, Tyrrell DL, Vederas JC, Lemieux MJ. 2020. Feline
501 coronavirus drug inhibits the main protease of SARS-CoV-2 and blocks virus replication.
502 Nat Commun 11:4282.

503 23. Wishart DS, Feunang YD, Guo AC, Lo EJ, Marcu A, Grant JR, Sajed T, Johnson D, Li C,
504 Sayeeda Z, Assempour N, Iynkkaran I, Liu Y, Maciejewski A, Gale N, Wilson A, Chin L,
505 Cummings R, Le D, Pon A, Knox C, Wilson M. 2018. DrugBank 5.0: a major update to the
506 DrugBank database for 2018. Nucleic Acids Res 46:D1074-D1082.

507 24. Pruijssers AJ, George AS, Schafer A, Leist SR, Gralinksi LE, Dinnon KH, 3rd, Yount BL,
508 Agostini ML, Stevens LJ, Chappell JD, Lu X, Hughes TM, Gully K, Martinez DR, Brown AJ,
509 Graham RL, Perry JK, Du Pont V, Pitts J, Ma B, Babusis D, Murakami E, Feng JY, Bilello
510 JP, Porter DP, Cihlar T, Baric RS, Denison MR, Sheahan TP. 2020. Remdesivir Inhibits
511 SARS-CoV-2 in Human Lung Cells and Chimeric SARS-CoV Expressing the SARS-CoV-
512 2 RNA Polymerase in Mice. Cell Rep 32:107940.

513 25. Capozzi M, De Divitiis C, Ottaiano A, von Arx C, Scala S, Tatangelo F, Delrio P, Tafuto S.
514 2019. Lenvatinib, a molecule with versatile application: from preclinical evidence to future
515 development in anti-cancer treatment. Cancer Manag Res 11:3847-3860.

516 26. Suyama K, Iwase H. 2018. Lenvatinib: A Promising Molecular Targeted Agent for Multiple
517 Cancers. Cancer Control 25:1073274818789361.

518 27. Kneller DW, Phillips G, O'Neill HM, Jedrzejczak R, Stols L, Langan P, Joachimiak A,
519 Coates L, Kovalevsky A. 2020. Structural plasticity of SARS-CoV-2 3CL M(pro) active site
520 cavity revealed by room temperature X-ray crystallography. Nat Commun 11:3202.

521 28. Majeux N, Scarsi M, Caflisch A. 2001. Efficient electrostatic solvation model for protein-
522 fragment docking. Proteins 42:256-68.

523 29. Majeux N, Scarsi M, Apostolakis J, Ehrhardt C, Caflisch A. 1999. Exhaustive docking of
524 molecular fragments with electrostatic solvation. Proteins 37:88-105.

525 30. Scarsi M, Apostolakis J, Caflisch A. 1997. Continuum electrostatic energies of
526 macromolecules in aqueous solutions. Journal of Physical Chemistry A 101:8098-8106.

527 31. MacKerell AD, Bashford D, Bellott M, Dunbrack RL, Evanseck JD, Field MJ, Fischer S,
528 Gao J, Guo H, Ha S, Joseph-McCarthy D, Kuchnir L, Kuczera K, Lau FTK, Mattos C,
529 Michnick S, Ngo T, Nguyen DT, Prodhom B, Reiher WE, Roux B, Schlenkrich M, Smith
530 JC, Stote R, Straub J, Watanabe M, Wiorkiewicz-Kuczera J, Yin D, Karplus M. 1998. All-
531 atom empirical potential for molecular modeling and dynamics studies of proteins. Journal
532 of Physical Chemistry B 102:3586-3616.

533 32. MacKerell AD, Jr., Feig M, Brooks CL, 3rd. 2004. Improved treatment of the protein
534 backbone in empirical force fields. J Am Chem Soc 126:698-9.

535 33. Vanommeslaeghe K, Hatcher E, Acharya C, Kundu S, Zhong S, Shim J, Darian E,
536 Guvench O, Lopes P, Vorobyov I, MacKerell AD. 2010. CHARMM General Force Field: A

537 Force Field for Drug-Like Molecules Compatible with the CHARMM All-Atom Additive
538 Biological Force Fields. Journal of Computational Chemistry 31:671-690.

539 34. Zhao HT, Huang DZ. 2011. Hydrogen Bonding Penalty upon Ligand Binding. Plos One 6.

540 35. Busnadiego I, Fernbach S, Pohl MO, Karakus U, Huber M, Trkola A, Stertz S, Hale BG.
541 2020. Antiviral Activity of Type I, II, and III Interferons Counterbalances ACE2 Inducibility
542 and Restricts SARS-CoV-2. mBio 11.

543 36. Konig R, Chiang CY, Tu BP, Yan SF, DeJesus PD, Romero A, Bergauer T, Orth A, Krueger
544 U, Zhou Y, Chanda SK. 2007. A probability-based approach for the analysis of large-scale
545 RNAi screens. Nat Methods 4:847-9.

546

Figure 1

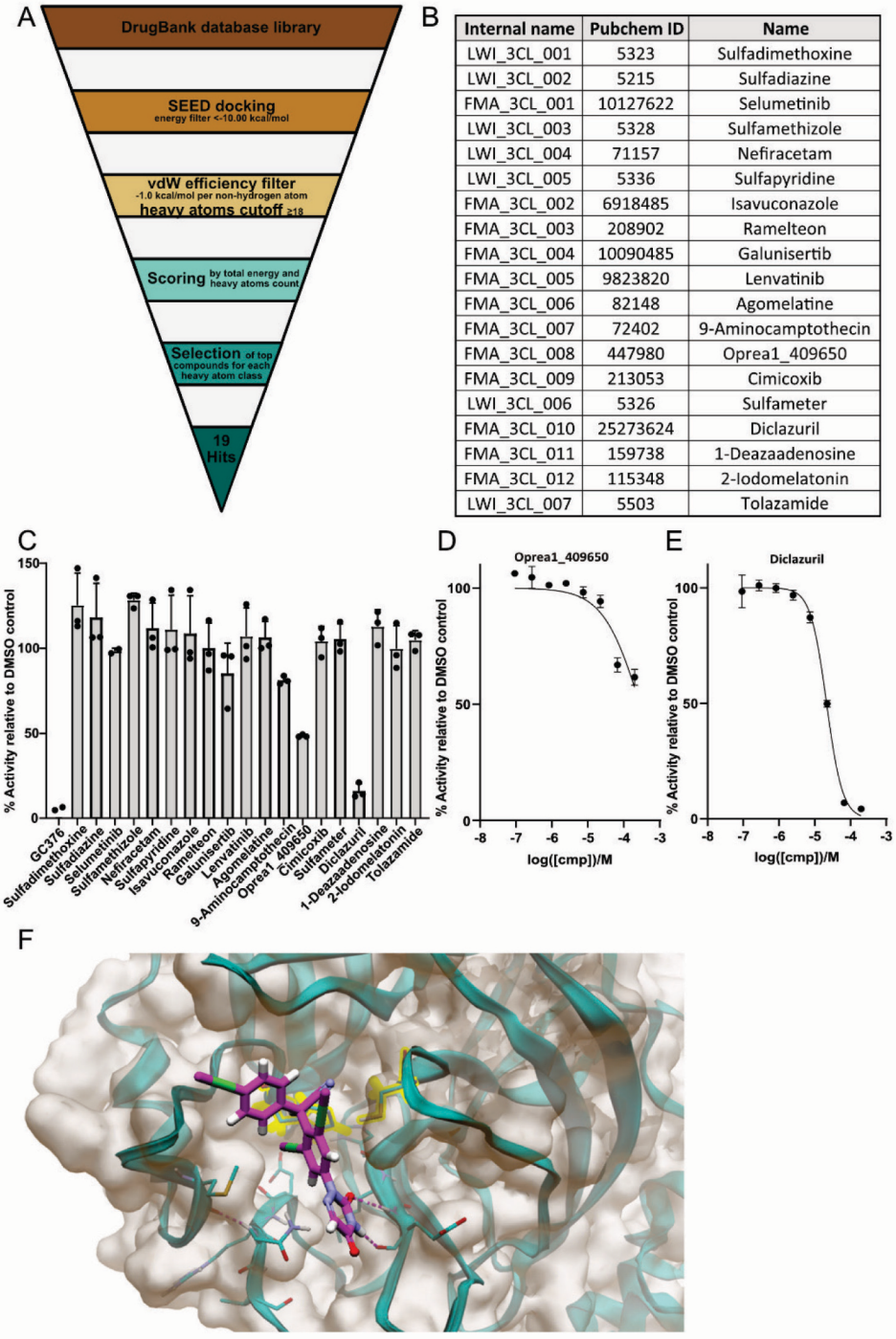

Internal name	Pubchem ID	Name
LWI_3CL_001	5323	Sulfadimethoxine
LWI_3CL_002	5215	Sulfadiazine
FMA_3CL_001	10127622	Selumetinib
LWI_3CL_003	5328	Sulfamethizole
LWI_3CL_004	71157	Nefiracetam
LWI_3CL_005	5336	Sulfapyridine
FMA_3CL_002	6918485	Isavuconazole
FMA_3CL_003	208902	Ramelteon
FMA_3CL_004	10090485	Galunisertib
FMA_3CL_005	9823820	Lenvatinib
FMA_3CL_006	82148	Agomelatine
FMA_3CL_007	72402	9-Aminocamptothecin
FMA_3CL_008	447980	Oprea1_409650
FMA_3CL_009	213053	Cimicoxib
LWI_3CL_006	5326	Sulfameter
FMA_3CL_010	25273624	Diclazuril
FMA_3CL_011	159738	1-Deazaadenosine
FMA_3CL_012	115348	2-Iodomelatonin
LWI_3CL_007	5503	Tolazamide

Figure 2

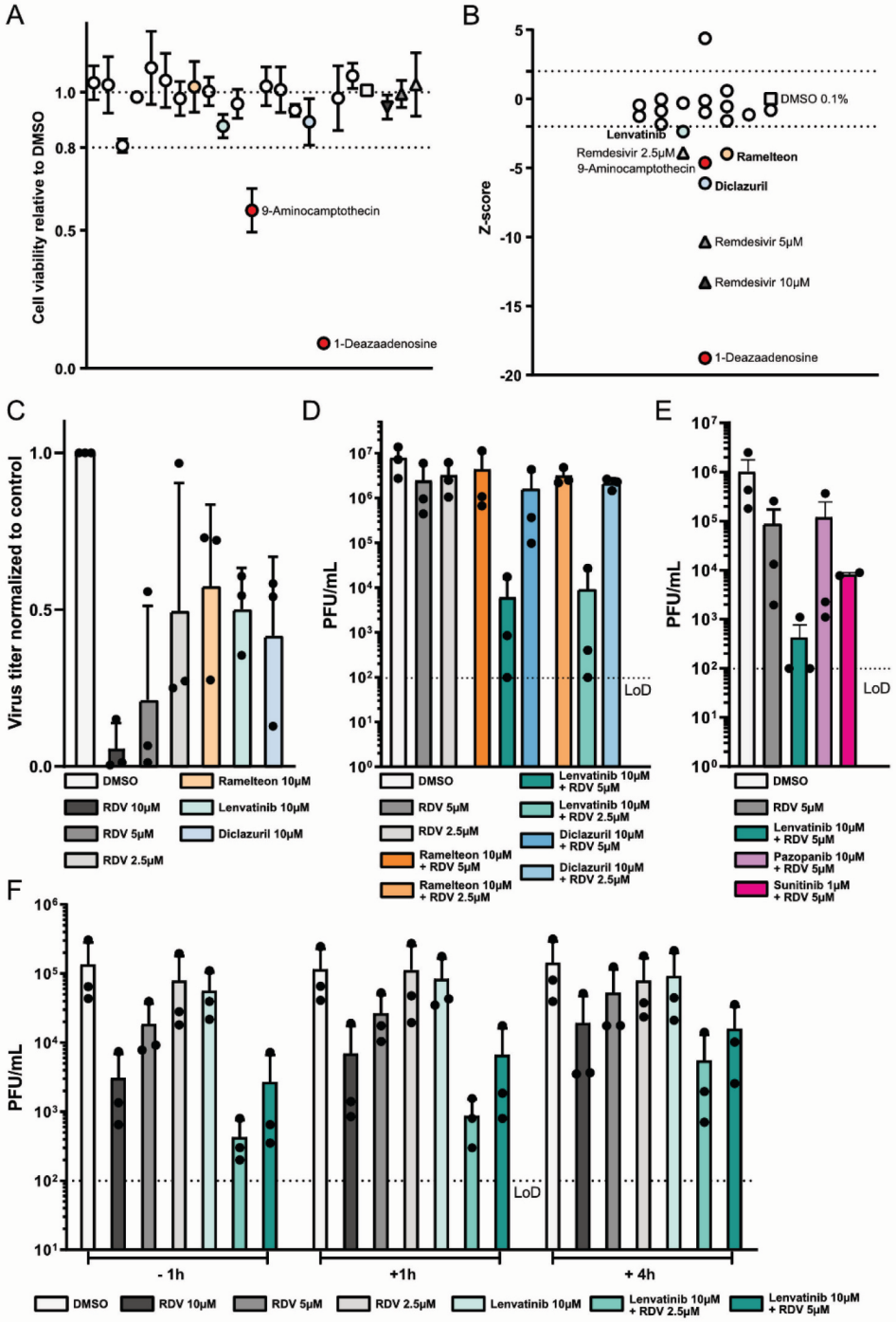
A
Cell viability relative to DMSO
1.0
0.8
0.5
0.0
9-Aminocamptothecin
1-Deazaadenosine
B
Z-score
5
0
-5
-10
-15
-20
DMSO 0.1%
Lenvatinib
Remdesivir 2.5μM
9-Aminocamptothecin
Ramelteon
Diclazuril
Remdesivir 5μM
Remdesivir 10μM
1-Deazaadenosine
C
Virus titer normalized to control
1.0
0.5
0.0
DMSO
RDV 10μM
RDV 5μM
RDV 2.5μM
Ramelteon 10μM
Lenvatinib 10μM
Diclazuril 10μM
D
PFU/mL
LoD
DMSO
RDV 5μM
RDV 2.5μM
Ramelteon 10μM + RDV 5μM
Ramelteon 10μM + RDV 2.5μM
Lenvatinib 10μM + RDV 5μM
Lenvatinib 10μM + RDV 2.5μM
Diclazuril 10μM + RDV 5μM
Diclazuril 10μM + RDV 2.5μM
E
PFU/mL
LoD
DMSO
RDV 5μM
Lenvatinib 10μM + RDV 5μM
Pazopanib 10μM + RDV 5μM
Sunitinib 1μM + RDV 5μM
F
PFU/mL
LoD
- 1h
+1h
+ 4h
DMSO
RDV 10μM
RDV 5μM
RDV 2.5μM
Lenvatinib 10μM
Lenvatinib 10μM + RDV 2.5μM
Lenvatinib 10μM + RDV 5μM